Available online at www.sciencedirect.com
ScienceDirect
Journal of Solid State Chemistry 180 (2007) 2916–2925
JOURNAL OF SOLID STATE CHEMISTRY
www.elsevier.com/locate/jssc

# Rapid and exothermic solid-state synthesis of metal oxyhalides and their solid solutions via energetic metathesis reactions

Sujith Perera, Nadiya A. Zelenski, Randy E. Pho, Edward G. Gillan*

*Department of Chemistry and Nanoscience and Nanotechnology Institute, University of Iowa, 481 Chemistry Building, Iowa City, Iowa 52242, USA*

Received 28 June 2007; received in revised form 4 August 2007; accepted 6 August 2007
Available online 24 August 2007

**Abstract**

Rapid solid-state metathesis reaction chemistry has been extended to the production of layered metal oxyhalide systems. This article describes the successful synthesis of crystalline Bi*OX* (*X* = Cl, I), and lanthanide oxychlorides (*Ln*OCl, *Ln* = La, Sm, Gd) from metal trihalides and $Na_2O_2$ in seconds. These known materials contain halide double layers separating *M*–O layers. Powder X-ray diffraction results on the metathesis metal oxyhalide products agree with prior literature reports. The morphological and compositional properties of the metal oxyhalide products are described. The rapid production of well-mixed paramagnetic $Gd_xSm_{1-x}OCl$ solid-solution materials was achieved using physical mixtures of $SmCl_3$ and $GdCl_3$ precursors reacted with $Na_2O_2$. The room-temperature magnetic properties of these materials with varying compositions are also described. As expected, magnetism, unit cell parameters, and M–O vibrational bands are all dependent on metal composition in the solid-solution products and vary in an approximately linear Vegard's law fashion.


*Keywords:* Energetic chemistry; Solid-state metathesis; Metal oxyhalide; Magnetic material

## 1. Introduction

Low-dimensional solid-state materials often exhibit unusual anisotropic physical and chemical properties. Many layered solid-state structures also undergo insertion reactions between layers (intercalation) that can alter their electronic and magnetic properties. Classic examples include graphite and metal chalcogenide systems [1]. Several recent studies have shown that tailored layered metal oxides result in structural and magnetic changes [2]. Layered metal oxyhalides are another interesting anisotropic metal oxide system, where $MO_x$ layers are separated from each other by one or more layers of halide anions. Several well-studied examples crystallize in *MOX* compositions, such as main group Bi*OX* (*X* = Cl, Br, I) and lanthanide *Ln*OCl (*Ln* = La to Ho) structures. Many of these layered oxyhalides crystallize into a tetragonal unit cell ($D_{4h}$ symmetry) [3] with the tetragonal PbFCl-type structure (Fig. 1) [4]. This structure has an apparent layered arrangement with a chloride double layer separating the metal oxide layer; however in lanthanide systems, the metal's distance to chlorides in both "layers" is similar. Thus, this structure type is regarded as tightly bonded and difficult to intercalate. Though there are recent reports of anion exchange in Bi*OX* structures [5], related SmSI or YOF structures observed for heavier *M*OCl lanthanide oxychlorides have different halide arrangements and are more easily intercalated [6].

Bismuth oxyhalides, especially BiOCl, are used as pigments in the cosmetic industry [7], in oxidative cracking of *n*-butane [8], and more recently as UV or visible light photocatalysts and transparent nanocomposites [9]. Bismuth oxyhalides are commonly synthesized via aqueous precipitation of bismuth cations from a chloride solution using dissolved bismuth reagents such as $Bi_2O_3$ or $BiNO_3$ [9a,9c,10]. Nanosized bismuth oxyhalides have also been prepared via reverse microemulsions [9b]. Lanthanide oxyhalides show catalytic activity in the oxidative coupling of methane and cracking of *n*-butane [8,11], and have demonstrated gas sensing capabilities [12]. The *Ln*OCl lattice is able to accommodate luminescent rare earth

*Corresponding author. Fax: +1 319 335 1270.
*E-mail address:* edward-gillan@uiowa.edu (E.G. Gillan).

0022-4596/$ - see front matter © 2007 Elsevier Inc. All rights reserved.
doi:10.1016/j.jssc.2007.08.005

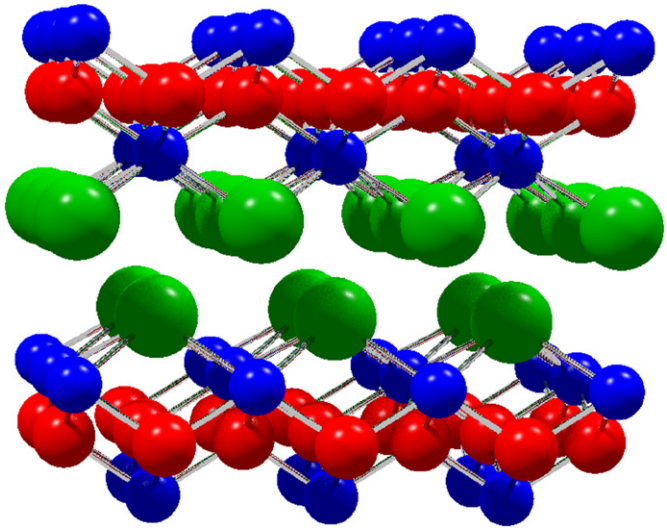

Fig. 1. Representation of the tetragonal structure of BiOCl. The $Bi^{3+}$ ions are blue (small black), $O^{2-}$ are red (dark grey), and $Cl^{-}$ are green (large light grey).

dopants and has application as commercial phosphor materials in CRT displays [13]. Conventional *Ln*OCl synthesis methods involve $Ln_2O_3$ reactions with $NH_4Cl$ [4c,14] or $Cl_2$ [15] at elevated temperatures or $LnCl_3$ reactions with water vapor or hydrated HCl vapor [4b,16]. Direct thermal reactions between $Ln_2O_3$ and $LnCl_3$ have also been reported [17]. All of these methods require high temperatures and need at least several hours of reaction time. One report describes a low temperature (300 °C) two-step *Ln*OCl synthesis, first producing an ammonium lanthanide chloride from the lanthanum oxide then converting it to *Ln*OCl using water vapor at 300 °C, but it required ~12 days of reaction time [6]. Subsequent alkali chloride flux crystallization at 450 °C was needed to improve product crystallinity. The high-energy mechanochemical synthesis of LaOCl using $La_2O_3$ and $LaCl_3$ has been also reported [18].

In the present study, we examine rapid exothermic solid-state metathesis (SSM) reactions for direct metal oxyhalide synthesis. Highly exothermic and self-propagating SSM reactions form a halide salt byproduct and usually release sufficient energy to melt the salt ($T > 1000$ °C). They are briefly analogous to flux-assisted solid-state syntheses and crystallization methodologies [19], but have a short window of a few seconds for significant atom diffusion and crystallization to occur. This method has been successfully used to synthesize crystalline pnictides, silicides, borides, chalcogenides, and oxides from metal halides and alkali metal or alkaline earth non-metal reagents in a generally rapid and exothermic manner [20,21]. Several furnace heated SSM-style precursor reactions (some with rapid initiation) produce mixed metal oxides and others produce porous complex oxide materials [22]. One study, particularly applicable to our current rapid SSM experiments, heated $LaCl_3/Li_2O$ mixtures to 500 °C for 10 h and showed evidence of partial LaOCl formation along with significant $La_2O_3$ formation [23]. The report below describes successful SSM reactions to form crystalline *MOX* materials in seconds. Examples of this method include BiOCl and BiOI, LaOCl, SmOCl, GdOCl, and several Sm/Gd solid-solution *M*OCl products. The compositional, morphological, and room-temperature magnetic properties of the synthesized layered metal oxyhalides are described.

## 2. Experimental section

### 2.1. Starting materials

The following solid reagents were used as-received for the synthesis of metal oxyhalides. $BiCl_3$ (Aldrich, 98 + %), $BiI_3$ (Aldrich 99.9%), $LaCl_3$ (Strem, anhydrous 99.9%—La, REO), $SmCl_3$ (Strem, anhydrous 99.9%—Sm, REO) or $GdCl_3$ (Strem, anhydrous 99.9%—Gd, REO), $Na_2O_2$ (Alfa Aesar, 93% min.), and $Na_2O$ (Aldrich, 97%). Methanol (Fisher Scientific, ACS grade) was used for post-reaction washing to remove byproduct salts and unreacted starting materials.

*Safety note*: SSM reactions have been known to initiate upon grinding solid reagents together, so care should be taken whenever investigating a new reactant pairing. For example, previous work showed that a $TiCl_3/Na_2O$ reaction can be initiated with a red-hot flash if it is vigorously ground for ~10 min with mortar and pestle [21e]. In the current study, one vigorously ground $LaCl_3/Na_2O$ precursor mixture also self-initiated in the glovebox. SSM reactions should be performed on small scales in reactors with pressure release options.

### 2.2. SSM synthesis of crystalline MOX materials

The following separate reagent pairs were used for the synthesis of different metal oxyhalide systems. For BiOCl:$BiCl_3$ (0.500 g, 1.58 mmol) and $Na_2O_2$ (0.124 g, 1.58 mmol); for BiOI:$BiI_3$ (0.500 g, 0.85 mmol) and $Na_2O_2$ (0.661 g, 0.85 mmol); for LaOCl:$LaCl_3$ (1.000 g, 4.08 mmol) and $Na_2O_2$ (0.318 g, 4.08 mmol) or $Na_2O$ (0.253 g, 4.08 mmol); for SmOCl:$SmCl_3$ (1.000 g, 3.89 mmol) and $Na_2O_2$ (0.304 g, 3.89 mmol); and for GdOCl:$GdCl_3$ (1.000 g, 3.79 mmol) and $Na_2O_2$ (0.296 g, 3.79 mmol). The molar ratio of metal trihalides to $Na_2O_x$ ($x = 1$ or 2) is 1:1 to ensure that all sodium is ideally sequestered as sodium halide in the product. In all cases, the metal halide was separately ground to a fine powder before being ground and mixed with the sodium–oxygen reagent, with all manipulations taking place in an inert atmosphere (argon) glovebox. In the solid-solution Gd/Sm oxychloride ($Gd_xSm_{1-x}OCl$) synthesis, $GdCl_3$:$SmCl_3$ relative molar ratios of 0.25:0.75 (0.250 g, 0.95 mmol:0.730 g, 2.84 mmol), 0.50:0.50 (0.500 g, 1.89 mmol:0.487 g, 1.89 mmol), and 0.75:0.25 (0.750 g, 2.84 mmol:0.243 g, 0.95 mmol) were used as metal halide precursor mixtures. The oxygen precursor, $Na_2O_2$ (0.296 g, 3.79 mmol), was used so that the molar

ratio of total metal trihalide to $Na_2O_2$ remained 1:1. For each Gd/Sm chloride mixture, the two metal trihalide reagents were ground separately, then intimately ground together, and finally ground together with $Na_2O_2$.

For each of the reagent mixtures described above, the metal halide/sodium peroxide or oxide reagent mixture was loaded in a ceramic crucible that was placed in a custom-built steel filament ignition reactor [24]. The reactor was sealed with its screw cap and removed from the glovebox. The exothermic reactions were initiated using a straight or coiled nichrome filament. The coiled filament consisted of ~10 loops of a 24 gauge (~0.5 mm) nichrome wire that was formed using a 2 mm diameter rod template. This coiled filament provides multiple initiation sites in the precursor powder mixture and aids in generating self-sustaining reactions in systems with high activation barriers [21e]. After the completed SSM reactions cooled to room temperature, the solid products were stirred in methanol (~80 ml for 1 g of as-synthesized product) for 30 min to remove any unreacted starting materials and sodium halide byproducts. The washed solid was isolated using vacuum filtration and then dried in an oven at 140 °C.

### 2.3. Characterization of synthesized *MOX* powders

The solid products were ground to a fine powder with mortar and pestle. The phase and crystallinity of the products were analyzed by powder X-ray diffraction (XRD) using a Siemens D5000 diffractometer (50 kW, 30 mA, 0.05–0.02°/steps and 1–6 s/step count times). Phase identification was made using reference data from the JCPDS database. A crystalline silicon powder internal standard consisting of a finely ground single-crystal silicon wafer (>99.9%) was used as a reference for lattice parameter calculations using Powder Cell 2.3 computer program (http://www.ccp14.ac.uk/) for *M*OCl solid-solution products. XRD pattern positions for the Gd/Sm solid-solution systems were normalized with respect to an internal Si standard to overcome any sample height or instrumentation errors since GdOCl and SmOCl have similar tetragonal unit cell *a* and *c* parameters. Infrared spectra were taken on a Nicolet Nexus 670 spectrometer in transmission mode using KBr pellets containing dilute products. Scanning electron microscopy (SEM) information was obtained with a Hitachi S-4000 or S-3400N field emission system (5 kV) on powders affixed to aluminum holders with carbon tape. The S-3400N system includes Si(Li) detector system for energy dispersive spectroscopy (EDS) (20 kV), that provided semiquantitative information on relative amounts of metal, sodium, and chlorine in the samples. Room-temperature magnetic susceptibility measurements were obtained on a Johnson–Matthey MKS-Auto (Mark II) benchtop magnetic susceptibility balance. Highly magnetic gadolinium-containing samples were diluted with a known amount of finely ground NaCl prior to analysis, otherwise they were attracted to the applied magnetic field too strongly and measurements were out of the range of the instrument. The *M*OCl results were calculated after subtracting diamagnetic NaCl components (if applicable) from the raw gram susceptibility data. In all cases a $5.8 \times 10^{-5}$ cm$^3$/mol *M*OCl diamagnetic correction was applied to the data [25]. Theoretical paramagnetic magnetic moments for the Gd/Sm solid-solution *M*OCl products were calculated based on a sum of individual magnetic moments for the relative amounts of each paramagnetic free metal ion ($M^{3+}$) present in the ideal $Gd_xSm_{1-x}OCl$ formula unit. Magnetic moment estimations from experimental 298 K molar susceptibilities were made using the ideal Curie paramagnetic formula [$\mu_{exp} = 2.83(\chi T)^{1/2}$ where $\chi$ is the corrected molar susceptibility].

## 3. Results and discussion

### 3.1. Structural analysis of *MOX* layered products

In the current study, the conversion of $MX_3$ reagents ($MX_3$ = $BiCl_3$, $BiI_3$, $LaCl_3$, $SmCl_3$, or $GdCl_3$) quickly into crystalline *MOX* structures (BiOCl, BiOI, LaOCl, SmOCl, or GdOCl) via exothermic reactions with $Na_2O_2$ was achieved. In these oxyhalide reactions, the formation of a stable alkali halide byproduct drives a successful rapid SSM (exchange) reaction. The ideal balanced generic reaction of $MX_3$ with $Na_2O_2$ is shown in Eq. (1) and relevant thermodynamic reaction information is contained in Table 1:

$$MX_3 + Na_2O_2 \rightarrow MOX + 2NaX + 0.5O_2 \quad (1)$$

In the case of BiOCl synthesis, a heated filament initiated a self-sustaining reaction between $BiCl_3$ and $Na_2O_2$, then the reactor's walls became hot to the touch and a gray–white vapor evolved from under the reactor's lid. Once the reaction was cooled to room temperature, a mainly fused white-tan mass remained at the bottom of the reactor with about a third of the solid splattered on the walls. The washed $BiCl_3$ reaction product is off-white and powder XRD data show that it is crystalline tetragonal BiOCl (JCPDS #06-0249, Fig. 2a) that compares well to a calculated BiOCl pattern (Fig. 2b). Based on a BiOCl product, the chemical yield is 38% (see Table 2), which may be low because of $BiCl_3$ vaporization loss due to its low melting and boiling points (Table 1) [26]. Given that $BiI_3$ has a higher melting/decomposition point than $BiCl_3$, an analogous reaction was attempted between $BiI_3$ and

Table 1
Thermodynamic data on metal trihalides and their reactions with $Na_2O_2$ to form oxyhalides

| Compound | $BiCl_3$ | $BiI_3$ | $LaCl_3$ | $SmCl_3$ | $GdCl_3$ |
|---|---|---|---|---|---|
| Melting pt. (°C) | 230 | 409 | 859 | 682 | 609 |
| $\Delta H_f$ (kJ/mol) | −287 | −16 | −1072 | −1026 | −1027 |
| $\Delta H_{rxn}$ (kJ/mol)[a] | −325 | −316 | −257 | −282 | −264 |

[a]Based on balanced reaction shown in Eq. (1).

$Na_2O_2$. This reaction also initiated, yielding a dark orange product after washing. The XRD of this material has very broad peaks that are consistent with tetragonal BiOI (JCPDS #10-0445, Fig. S1, electronic supporting material). The calculated yield was higher (56%) than the $BiCl_3$ reaction; however the product's poor crystallinity precluded more in depth study of the BiOI product.

Compared with bismuth trihalides, the lanthanide trichlorides examined in this study ($LaCl_3$, $SmCl_3$, and $GdCl_3$) have much higher melting points and therefore required coiled filaments to initiate a self-propagating reaction between themselves and $Na_2O_2$. In general, melting points of the lanthanide trichlorides decrease from $LaCl_3$ to $GdCl_3$ (Table 1) [27]. To achieve a successful propagating reaction for $LaCl_3$, a higher voltage was applied to the coiled filament than that needed for the lower melting $SmCl_3$ and $GdCl_3$ (Table 2). In these $Na_2O_2$ reactions, the crucible container became hot to the touch and after cooling it to room temperature, a mainly loose powdery white product mass was on the bottom of the reactor. After washing away the NaCl byproduct, the remaining white solids have XRD patterns (Fig. 2c,e,f) consistent with the tetragonal metal oxyhalide structures LaOCl (JCPDS #08-0477), SmOCl (JCPDS #12-0790), and GdOCl (JCPDS #12-0798) that compare well to a calculated LaOCl pattern (Fig. 2d). These coiled wire initiated SSM reactions have isolated *M*OCl yields above 60%. Previous literature studies on *Ln*OCl systems determined that the decomposition properties of *M*OCl products show similar overall trends to those noted above for $LnCl_3$ melting points. The lanthanide oxychlorides readily decompose to corresponding oxides with $MCl_3$ loss at about 1320, 1110, and 1090 °C for LaOCl, SmOCl, and GdOCl, respectively [28], though heating for hours at lower temperatures (~800 °C) also causes *M*OCl decomposition in some cases [29]. While the current SSM reactions may reach transient temperatures near the NaCl boiling point of ~1400 °C, the NaCl byproduct will absorb and dissipate heat to the container walls and quickly cool the reaction below the NaCl melting point (801 °C).

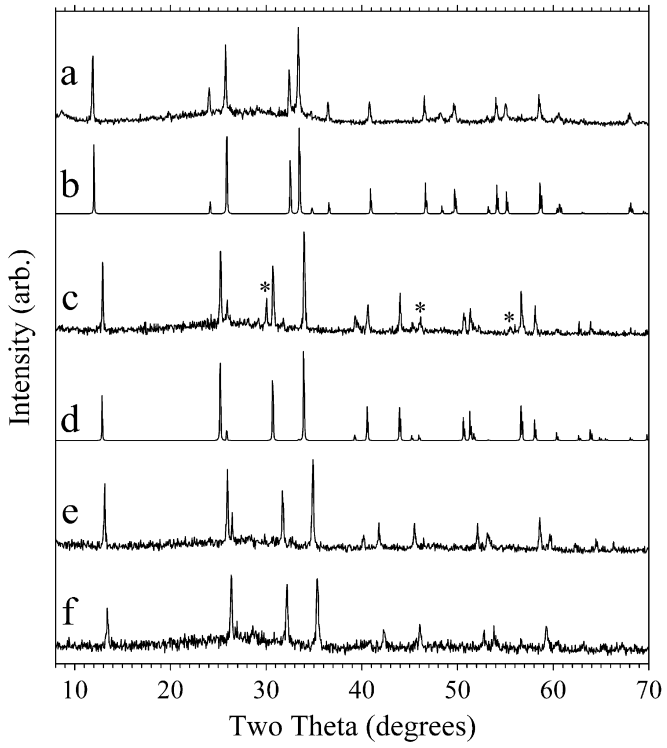


Fig. 2. XRD stack plot of the washed products from SSM reaction of $Na_2O_2$ with (a) $BiCl_3$, (c) $LaCl_3$, (e) $SmCl_3$, and (f) $GdCl_3$. The (*) labels denote $La_2O_3$ and all other peaks agree with MOCl structures. Simulated MOCl patterns are included for (b) BiOCl (tetragonal $a = 3.891$ Å, $c = 7.369$ Å) and (d) LaOCl (tetragonal $a = 4.119$ Å, $c = 6.883$ Å).

In the LaOCl SSM reaction, a small amount of $La_2O_3$ was also observed. $La_2O_3$ formation from $LaCl_3/Li_2O$ SSM reactions has been reported [23], so perhaps local stoichiometric inhomogeneities may contribute to some oxide formation. Since a higher thermal energy is needed for the initiation of the LaOCl precursor mixture, unreacted metal halide starting material may also remain and react during the washing process with available oxygen sources to form crystalline LaOCl and $La_2O_3$. Previous research has shown that $LaCl_3$, $SmCl_3$, and $GdCl_3$ will react directly with (heated) water vapor to liberate HCl and form the corresponding *M*OCl structures [16], thus it was important to determine whether crystalline *M*OCl could form via direct solution reactions between dissolved $MCl_3$ and $Na_2O_2$ during the methanol wash process. A control experiment was performed with separately dissolved/decomposed $LaCl_3$ and $Na_2O_2$ in methanol. These were mixed together and stirred in similar manner to that used in the SSM reaction washing process. The reagent amounts used were also similar to the LaOCl SSM reaction. XRD of the isolated products shows only amorphous material confirming that crystalline LaOCl forms during our

Table 2
Synthetic and structural data for SSM synthesized metal oxyhalides

| Compound | Filament type (voltage applied) | Yield[a] (%) | Lattice parameters (Å) PbFCl type, $P4/nmm$ (1 2 9) | *M*:Cl:Na molar ratio[b] |
|---|---|---|---|---|
| BiOCl | Straight (15 V) | 38 | $a = 3.890$, $c = 7.364$ | 1:0.78:0.03 |
| LaOCl | Coiled (20 V) | 73 | $a = 4.120$, $c = 6.882$ | 1:0.84:0.05 |
| SmOCl | Coiled (15 V) | 64 | $a = 3.982$, $c = 6.724$ | 1:0.75:0.05 |
| GdOCl | Coiled (15 V) | 61 | $a = 3.953$, $c = 6.668$ | 1:0.65:0.08 |

[a]Yield calculated based on *MOX* after washing away NaCl.
[b]From EDS; molar ratio normalized to metal (*M*).

exothermic SSM reaction and the oxide side product is not a consequence of reagent hydrolysis during the washing process.

As noted above, alkali oxides ($Li_2O$, $Na_2O$) have been successfully used in previous metal oxide SSM metathesis reactions [20,21]. The reaction of $LaCl_3$ with $Na_2O$ instead of $Na_2O_2$ was also examined to determine whether alternate solid oxygen sources are viable for rapid *M*OCl formation (Eq. (2)),

$$LaCl_3 + Na_2O \rightarrow LaOCl + 2NaCl \quad (2)$$

In contrast to the $Na_2O_2$ reaction, this $Na_2O$ reaction should have no $O_2$ byproduct formation and it also has a somewhat higher enthalpy of reaction (−351 kJ/mol versus −257 kJ/mol). The SSM reaction was carried out in the same manner as used for $LaCl_3/Na_2O_2$ and a white product remained in the crucible after the reaction. The product was washed with methanol and had higher yield (85% based on LaOCl) than the $Na_2O_2$ reaction product. While its XRD pattern shows mainly LaOCl, there was also clear $La(OH)_3$ present, but no $La_2O_3$ (see Fig. S2). Note that it has been reported that $La_2O_3$ and LaOCl will convert to $La(OH)_3$ in presence of water, thus a larger $La_2O_3$ byproduct formation or smaller LaOCl crystallites formed in the $Na_2O$ reaction may lead to $La(OH)_3$ appearance after reaction with atmospheric moisture [12,30].

The synthesis of LaOCl from this $Na_2O$ SSM reaction contrasts with previous SSM reactions between $LaCl_3$ and $Li_2O$ that were heated at 500 °C for 10 h and produced a nearly equivalent mixture of $La_2O_3$ and LaOCl. In our rapid SSM reactions, the quick heating/cooling cycle afforded by filament-initiated reactions may aid in quenching out an initially formed *Ln*OCl phase that is not given time to convert to the stable $Ln_2O_3$ structure. Note also that increased amounts of dissolved $O^{2-}$ in molten salt flux reactions are an important factor in $Ln_2O_3$ versus *Ln*OCl growth [31]. While molten NaCl is produced in these exothermic SSM reactions, there may not be enough time to achieve high dissolved oxygen concentrations that can occur in equilibrated furnace heated SSM reaction systems.

As noted in Section 2, one major reason for not pursuing a wider use of $Na_2O$ with metal halides, in spite of the apparent higher product yields noted above, is that more frequent self-initiation reactions were observed while grinding $Na_2O$ ($\Delta H_f = -418$ kJ/mol) precursor mixtures in the glovebox. We never observed unintended exothermic initiation events with the $Na_2O_2$ ($\Delta H_f = -513$ kJ/mol) reactions, thus on balance it is a safer solid oxygen source to use in SSM synthesis examined here. Also note that $Na_2O$ is impure and usually sold as a mixture of $Na_2O$ and $Na_2O_2$ and it costs twice as much as $Na_2O_2$. Other metal halides (e.g., bromides) and possibly other metal oxygen sources may also lead to MOX products via rapid SSM reactions, provided that the thermodynamics are sufficiently exothermic to allow rapid self-propagation. For example, stable $Na_2CO_3$ ($\Delta H_f = -1131$ kJ/mol) and $Na_2C_2O_4$ ($\Delta H_f = -1318$ kJ/mol) are less likely to form self-propagating exothermic reactions with stable lanthanide halides, though they may be successful in furnace heated SSM reactions. During a previous study [21e], the reaction of $TiCl_3$ with $Na_2CO_3$ to form $TiO_2$ was attempted, but could not be initiated with a heated filament.

### 3.2. Compositional analysis of MOX SSM products

The metal (*Ln* or Bi):halide:sodium relative atomic ratios obtained from EDS for the metal oxyhalide products are shown in Table 2. In the La, Sm, and Gd cases, their *M* emission lines overlap with the Na K line, which will cause an overestimation of the Na, *Ln*, or Bi amounts in the sample [32]. Sodium content is analyzed as 3–8% in Table 2 (relative to *M* in *MOX*), but this is an overestimation because the actual EDS spectra show little or no visible peak area in the Na K line region (see Fig. S3). For metal (*Ln* or Bi) analysis, the L line was used and for chlorine analysis its K line was used since they do not overlap with each other or the sodium K line [33]. The *Ln* or Bi to halogen ratio is slightly less than 1:1 in all SSM oxyhalide products. With all of the analysis caveats noted above, the consistently less than 1:1 metal (*Ln* or Bi) to chlorine ratios suggest that some metal oxide formation or post-reaction hydrolysis may occur in these layered *MOX* syntheses. In the BiOI system, no significant overlapping EDS lines were observed, but this poorly crystalline product also had less than a 1:1 bismuth to iodine ratio (supporting info). Since BiOI is known to decompose above 300 °C, partial decomposition may produce amorphous $Bi_2O_3$ and lower overall iodine content [26].

### 3.3. IR spectroscopic analysis of MOX products

The solid IR of the washed $BiCl_3$ SSM reaction product is consistent with the BiOCl lattice vibration reported at

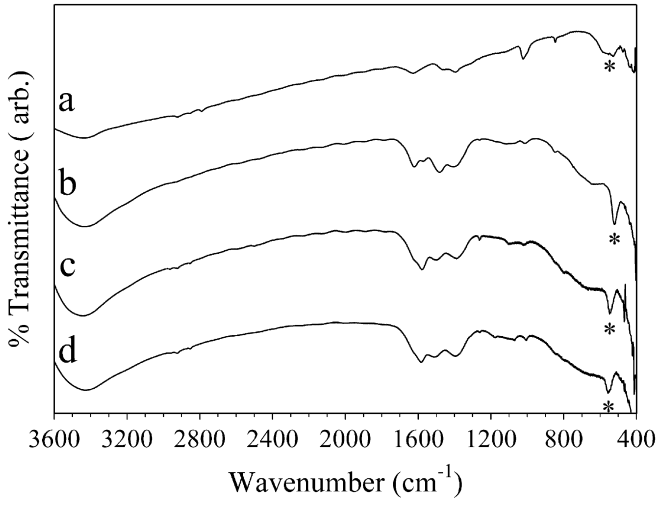


Fig. 3. Solid phase IR spectra of SSM products from reaction of $Na_2O_2$ with (a) $BiCl_3$, (b) $LaCl_3$, (c) $SmCl_3$, and (d) $GdCl_3$. The *M*–O lattice vibration in *M*OCl is identified with a (*).

528 $cm^{-1}$ (Fig. 3a) [3b,34]. The poorly crystalline BiOI also showed an identifiable BiOI lattice vibration at 488 $cm^{-1}$ (not shown). The characteristic IR spectral features for the lanthanide oxychlorides are intense around 515–550 $cm^{-1}$ and vibrational energies increase as lanthanide molar mass increases, as was observed in the previous work [3a]. The lanthanide oxychlorides show lattice vibrations for LaOCl at 520 $cm^{-1}$, SmOCl at 547 $cm^{-1}$, and GdOCl at 556 $cm^{-1}$ (Fig. 3b–d). There is no clear evidence for corresponding metal oxide ($M_2O_3$) lattice vibrations, which generally have their strongest IR vibrations about 20–30 $cm^{-1}$ lower than the observed IR peaks for each *M*OCl product [35]. There is notable broadening in the BiOCl vibration near 500 $cm^{-1}$ that may be due to amorphous $Bi_2O_3$ and some $La_2O_3$ (present in LaOCl sample based on Fig. 2 XRD) may be visible at the edge of our analysis window, since it reportedly has a strong vibration near 415 $cm^{-1}$ [35].

The IR spectra, particularly for the lanthanide oxychlorides, also show several broad peaks consistent with methanol vibrations (near 1000–1600, 2900, and 3500 $cm^{-1}$), though the intense vibrations in the ~1350–1600 $cm^{-1}$ are higher than those expected from free methanol (~1000–1400 $cm^{-1}$) [36]. It has been observed that when electron withdrawing groups are attached to the oxygen on methanol (e.g., $H_3CO$–F), its methyl deformation band is near 1500 $cm^{-1}$, which is higher than that for $CH_3OH$. This suggests that the methanol wash process may generate some strongly adsorbed methanol or facilitate surface reactions that leave methoxy substituents on the *MOX* particles. It is unlikely that methanol intercalates into the *MOX* structures to any appreciable extent since the *MOX* interlayer XRD peaks do not show any apparent shift relative to previously reported materials (Fig. 2). Partial hydrolysis of the *Ln*OCl surface sites by air-exposure or residual water in methanol to form terminal Ln–OH may also contribute to the higher energy absorptions in the 3400 $cm^{-1}$ spectral region.

### 3.4. *MOX morphology comparison*

From the well-crystallized XRD data shown earlier, one expects particle domains to approach micron sizes, which is verified by SEM results. The BiOCl product shows rough edged plate-like particles with 200–800 nm diameters (Fig. 4A). The LaOCl and SmOCl products have flat oval morphologies with smooth edges and with various diameters from ~100 nm to several microns (Fig. 4B and C). In the case of GdOCl, ~700–900 nm size jagged and irregular elongated plates and ~30 nm size particles represent its characteristic morphology. In previous reports, related plate-like or anisotropic morphologies have been observed for BiOCl [9a,10], LaOCl [30b], and SmOCl [15]. Consistent with its poorly crystallized XRD pattern, the BiOI product showed evidence of micron-sized layer like aggregations of ~70 nm particles (Fig. S4).

### 3.5. *Synthesis and analysis of solid-solution Sm/Gd oxychlorides*

Mixed metal solid-solution products have been produced from the rapid SSM reaction method via furnace or filament ignition using either physical mixtures of metal halides or solid-solution metal halides [37]. Given the rapid nature of SSM reactions, pre-mixing metal halide reagents is very important. We intimately ground individual metal

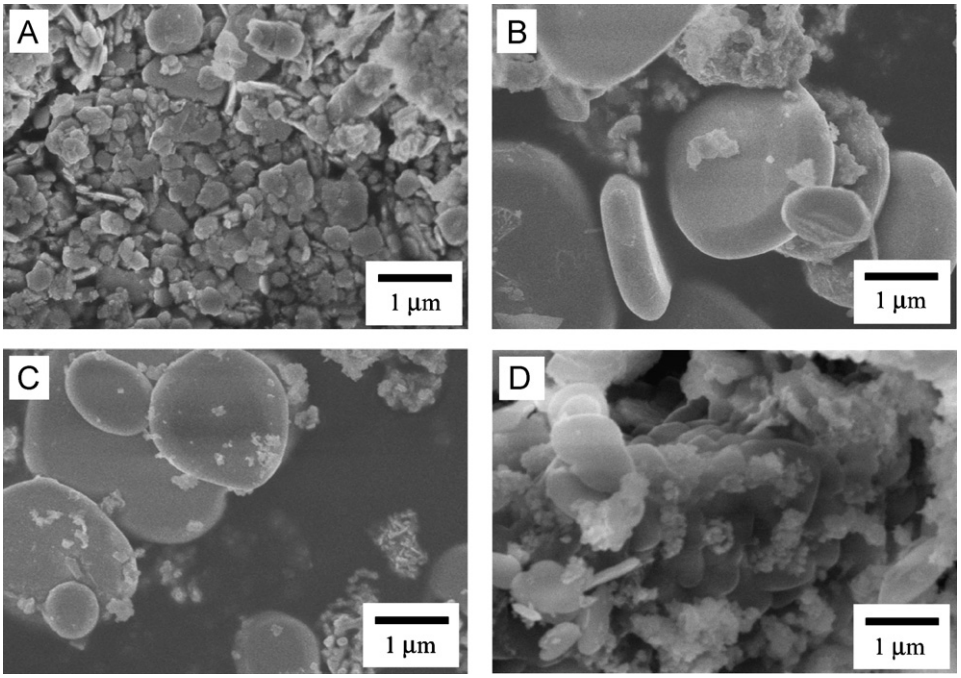


Fig. 4. SEM images of the washed SSM product from the reaction of $Na_2O_2$ and (A) $BiCl_3$, (B) $LaCl_3$, (C) $SmCl_3$, and (D) $GdCl_3$.

Table 3
Synthetic and structural data for SSM synthesized $Gd_xSm_{1-x}OCl$ solid solutions

| Ideal formula | Yield[a] (%) | Gd:Sm molar ratio[b] | (Gd + Sm):Cl molar ratio[b] | Lattice parameters (Å) PbFCl type, *P4/nmm* (1 2 9) | $\chi_m$ in $cm^3$/mol and $\mu_{exp}$ ($\mu_{calc}$) at 298 K |
|---|---|---|---|---|---|
| $Gd_{0.25}Sm_{0.75}OCl$ | 65 | 1:3.2 | 1:0.65 | $a = 3.978$, $c = 6.711$ | $5.82 \times 10^{-3}$ 3.72 $\mu_B$ (3.18) |
| $Gd_{0.50}Sm_{0.50}OCl$ | 60 | 1:0.99 | 1:0.73 | $a = 3.966$, $c = 6.691$ | $1.16 \times 10^{-2}$ 5.06 $\mu_B$ (4.77) |
| $Gd_{0.75}Sm_{0.25}OCl$ | 65 | 1:0.36 | 1:0.90 | $a = 3.963$, $c = 6.676$ | $1.46 \times 10^{-2}$ 5.91 $\mu_B$ (6.35) |

[a]Yield calculated based on $Gd_xSm_{1-x}OCl$ after washing away NaCl.
[b]From EDS; molar ratio normalized to total metal (Gd + Sm).

halides, $GdCl_3$ and $SmCl_3$, in various molar ratios and then mixed them with $Na_2O_2$ and performed a rapid SSM reaction as described below (Eq. (3)).

$$x\,GdCl_3 + (1-x)SmCl_3 + Na_2O_2 \rightarrow Gd_xSm_{1-x}OCl + 2NaCl + 0.5O_2 \quad (3)$$

The yields of $Gd_xSm_{1-x}OCl$ ($x = 0.25$, 0.5, and 0.75) SSM reaction products are similar to GdOCl and SmOCl yields (Tables 2 and 3). The lattice parameters for the tetragonal GdOCl and SmOCl end members are sensible since the radius of $Gd^{3+}$ is slightly smaller than $Sm^{3+}$. The washed and dried white solid-solution $Gd_xSm_{1-x}OCl$ product XRD patterns show a tetragonal structure very similar to GdOCl and SmOCl with peaks and lattice parameters that fall in between the single metal oxyhalide structures (Table 3). Fig. 5 shows stack plots for (1 1 0) and (1 0 2) peaks to illustrate the XRD peak shifts from larger to smaller unit cell dimensions as Gd content increases. The *M*OCl IR lattice vibration also shows peak shifts to lower energy as the gadolinium content decreases and the unit cell gets larger (Fig. S5). Note that low angle shoulders on some of the XRD peaks in Fig. 5 indicate that local stoichiometric inhomogeneities are present to some extent in these solid-solution $Gd_xSm_{1-x}OCl$ products. This is not surprising since the entire anion–cation metathesis/atom diffusion/product crystallization series of events in these rapid SSM reactions occurs in a few seconds. If the individual metal halides were not intimately mixed prior to reaction, it is likely that product inhomogeneity would be a much larger problem (i.e., regions of crystallized Gd-rich and Sm-rich phases). There are several ways to improve metal mixing in these solid-solution reactions ranging from the use of an atomically mixed solid-solution metal halide precursor (e.g., $Gd_xSm_{1-x}Cl_3$) or subjecting the isolated SSM reaction products to a post-reaction annealing heat treatment step. A third alternative would be to initiate the SSM reaction in an externally heated sealed ampoule, followed by longer term annealing [20a,22,23].

EDS atomic ratio data on $Gd_xSm_{1-x}OCl$ products show Gd:Sm ratios that compare well with molar ratios of reagents used, specifically Gd:Sm ratios of 1:3, 1:1, and 1:0.33 (Table 3). The metal (Gd + Sm) to Cl ratios are similar to the data for the single metal end members. The chlorine deficiency suggests that parts of the sample may be oxygen-rich, but no $M_2O_3$ phases were detected by XRD. EDS elemental mapping of the three different $Gd_xSm_{1-x}OCl$ systems show that both metals are evenly distributed in the bulk material down to the micron level and mirror the structural features shown in the SEM images (Fig. 6).

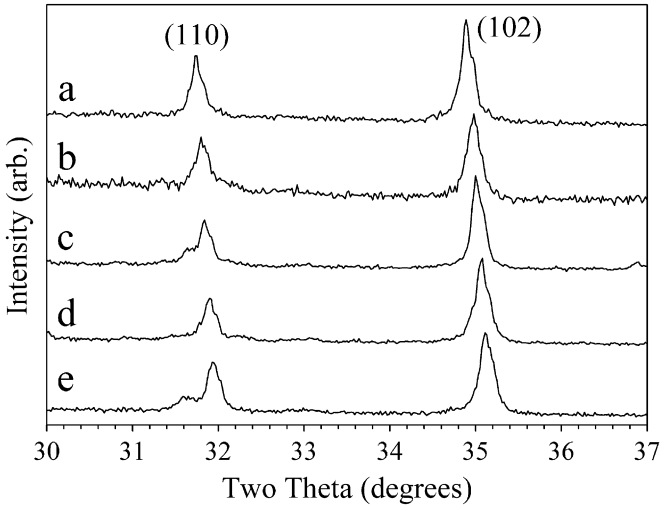


Fig. 5. XRD stack plot of (1 1 0) and (1 0 2) diffraction peaks for (a) SmOCl, (b) $Gd_{0.25}Sm_{0.75}OCl$, (c) $Gd_{0.50}Sm_{0.50}OCl$, (d) $Gd_{0.75}Sm_{0.25}OCl$, and (e) GdOCl.

Both of the SSM-synthesized SmOCl and GdOCl products are paramagnetic at room temperature and theoretically have five or seven unpaired electrons for their trivalent metal ions, $Sm^{3+}$ ($4f^5$) and $Gd^{3+}$ ($4f^7$). The calculated magnetic moments for $Sm^{3+}$ and $Gd^{3+}$ free ions are 1.60 and 7.94 $\mu_B$, when accounting for spin–orbit coupling and orbital mixing interactions [38]. The room-temperature molar magnetic susceptibility of SSM-synthesized SmOCl and GdOCl were measured to be $1.37 \times 10^{-3}$ and $2.03 \times 10^{-2}$ $cm^3$/mol, respectively. These values correspond to magnetic moments per $M^{3+}$ metal ion of 1.81 $\mu_B$ (SmOCl) and 6.96 $\mu_B$ (GdOCl), based on ideal Curie-type behavior at 298 K, which agree reasonably well with free ion values noted above. Previous reports on room-temperature molar magnetic susceptibility of SmOCl are in the $1 \times 10^{-3}$ $cm^3$/mol range and SmOCl shows evidence of an antiferromagnetic transition at 8 K [39]. The room-temperature magnetic moments of related *Ln*OBr materials

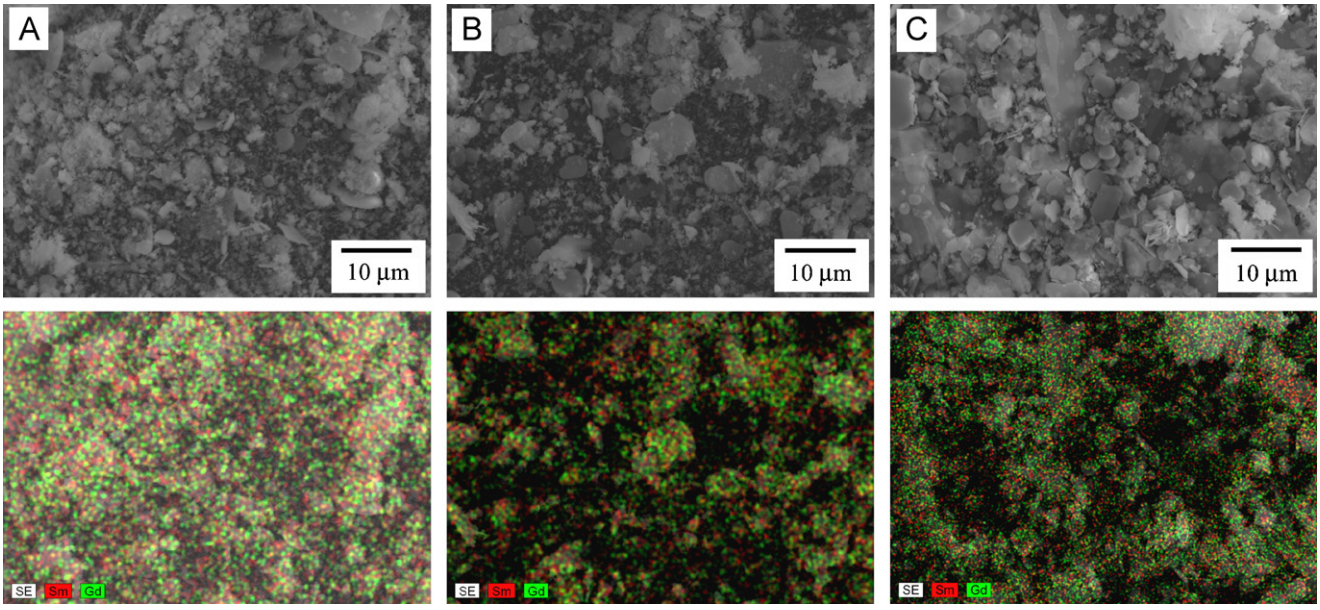


Fig. 6. SEM (top image) and corresponding EDS map of Gd and Sm distribution (bottom image) in the $Gd_xSm_{1-x}OCl$ solid-solution reaction products with (A) $x = 0.25$, (B) $x = 0.5$, and (C) $x = 0.75$. EDS images are overlays of SEM (white) with Sm (red, dark grey) and Gd (green, light grey) elemental signals.

for most of the lanthanide series are in good agreement with free metal-ion values ranging from 2.4 to 10.3 $\mu_B$, except SmOBr that was noted as being anomalously high [40]. Gadolinium molecular complexes are commonly used in magnetic resonance imaging (MRI) studies [41] and unusual Gd nanostructures show potential utility in MRI imaging, with one paper reporting 6.78 $\mu_B$/Gd for a Gd-filled/carbon nanotube [42]. Gadolinium is also a component in magnetically characterized oxides (7.93–7.99 $\mu_B$/Gd in $Sm_{2-x}Gd_xCuO_4$ solid solutions for $x = 1$–2, 7.68 $\mu_B$/Gd in $Gd_3[SiON_3]O$, and 8.37 $\mu_B$/Gd in $GdPO_4$) [43] and GdOCl serves as a host for luminescent $Eu^{3+}$ ions [44], but there are apparently no previous reports on the magnetic properties of GdOCl.

The room-temperature molar magnetic susceptibility values for the solid-solution $Gd_xSm_{1-x}OCl$ ($x = 0.25$, 0.5, and 0.75) powders were intermediate between those of SmOCl and GdOCl (Table 3). Their approximate magnetic moments agree reasonably well with calculated values assuming an ideal mixture of free ion $M^{3+}$ magnetic moments in the $Gd_xSm_{1-x}OCl$ samples. As expected, an increase in Gd content leads to more strongly magnetic *M*OCl structures. All of samples containing some gadolinium are sufficiently paramagnetic that they were visibly attracted to a permanent magnet through the walls of a glass vial. Graphical representations of the change in *a* and *c* lattice parameters and measured molar susceptibility versus ideal solid-solution composition are shown in Fig. 7. With the limited number of data points, an approximate Vegard's law linear change in both of these properties with composition is apparent. These mixed metal oxyhalides have not been previously reported, though GdOCl doped with 1% Sm was studied as an optical up-conversion laser material [45]. In future work, we will examine the local metal environment and variable temperature magnetic properties of these SSM-synthesized magnetic solid-solution layered *M*OCl structures.

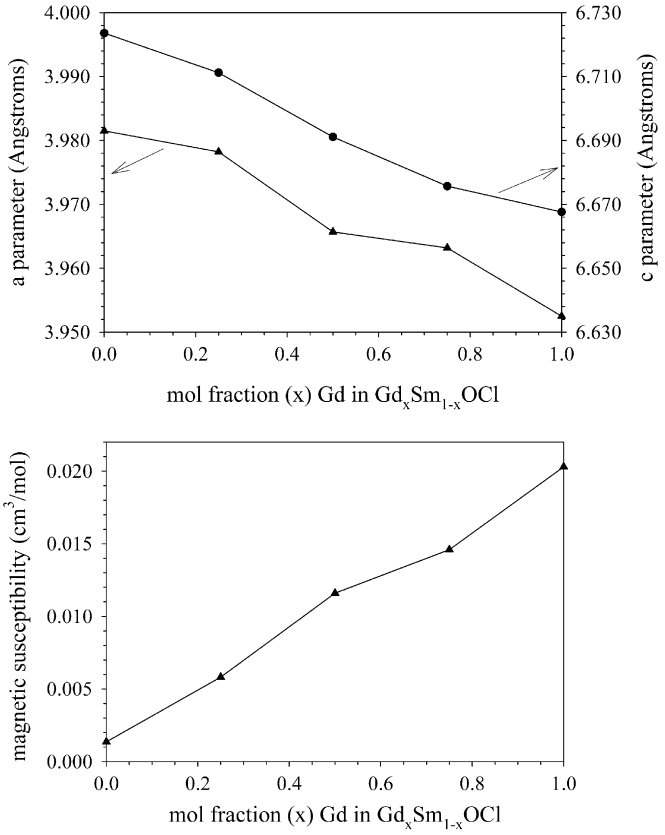


Fig. 7. Plots of $Gd_xSm_{1-x}OCl$ solid-solution results as a function of mole fraction Gd ($x$) for tetragonal unit cell *a* and *c* lattice parameters (top graph) and room-temperature molar magnetic susceptibility (bottom graph).

## 4. Conclusions

The rapid SSM energetic precursor route for the synthesis of oxide materials has been increased in scope to produce crystalline layered metal oxyhalides (*MOX*) from metal trihalides and sodium peroxide. By a judicious (and simple) change in reagent stoichiometries, *MOX* materials including BiO*X* ($X = Cl$ or I), LaOCl, SmOCl, and GdOCl are produced in seconds as microcrystalline solids with plate-like morphologies. We also obtained well-mixed, solid-solution $Gd_xSm_{1-x}OCl$ materials in a controlled manner using mixtures of the individual metal halides and $Na_2O_2$. The formation of solid-solution *MOCl* materials from these exothermic reactions that only last several seconds, is supported by XRD, IR, EDS elemental mapping, and room-temperature magnetic susceptibility data. The SSM reaction modifications that led to these successful *MOX* syntheses, may find use beyond oxides, to other layered nitrido- or sulfido-halide structures.

## Acknowledgments

The authors thank the National Science Foundation (CHE-0407753) and the University of Iowa MPSFP grant program for funding support.

## Appendix A. Supplementary data

Supplementary data associated with this article can be found in the online version at doi:10.1016/j.jssc.2007.08.005.

## References

[1] (a) A.J. Jacobson, in: A.K. Cheetham, P. Day (Eds.), Solid State Chemistry Compounds, Clarendon Press, New York, 1992, pp. 182–233 and references therein;
(b) D.W. Murphy, in: T.E. Mallouk (Ed.), Advances in the Synthesis and Reactivity of Solids, vol. 1, JAI Press Ltd., Greenwich, CT, 1991, pp. 237–272 and references therein.
[2] (a) L. Viciu, T.A. Kodenkandath, J.B. Wiley, J. Solid State Chem. 180 (2007) 583;
(b) D. Neiner, L. Spinu, V. Golub, J.B. Wiley, Chem. Mater. 18 (2006) 518 and references therein;
(c) D.G. Porob, P.A. Maggard, Chem. Mater. 19 (2007) 970 and references therein.
[3] (a) L.J. Basile, J.R. Ferraro, D. Gronert, J. Inorg. Nucl. Chem. 33 (1971) 1047;
(b) J.E.D. Davies, J. Inorg. Nucl. Chem. 35 (1973) 1531.
[4] (a) A.F. Wells, Structural Inorganic Chemistry, fifth ed., Clarendon Press, Oxford, 1990;
(b) D.H. Templeton, C.H. Dauben, J. Am. Chem. Soc. 75 (1953) 6069;
(c) L.H. Brixner, E.P. Moore, Acta Crystallogr. c39 (1983) 1316;
(d) J. Ketterer, V. Kraemer, Acta Crystallogr. c42 (1986) 1098.
[5] R.P. Bontchev, F. Bonhomme, J.L. Krumhansl, R.C. Moore, in: 229th ACS National Meeting, INOR 866, San Diego, CA, March 13–17, 2005.
[6] K. Song, S.M. Kauzlarich, Chem. Mater. 6 (1994) 386.
[7] (a) G. Pfaff, P. Reynders, Chem. Rev. 99 (1999) 1963;
(b) F.J. Maile, G. Pfaff, P. Reynders, Prog. Org. Coat. 54 (2005) 150.
[8] N. Kijima, K. Matano, M. Saito, T. Oikawa, T. Konishi, H. Yasuda, T. Sato, Y. Yoshimura, Appl. Catal. A: Gen. 206 (2001) 237.
[9] (a) K.-L. Zhang, C.-M. Liu, F.-Q. Huang, C. Zheng, W.-D. Wang, Appl. Catal. B 68 (2006) 125;
(b) J. Henle, P. Simon, A. Frenzel, S. Scholz, S. Kaskel, Chem. Mater. 19 (2007) 366;
(c) W. Wang, F. Huang, X. Lin, Scripta Mater. 56 (2007) 669.
[10] T.V. Daminova, M.N. Novokreshchenova, Y.M. Yukhin, Russ. J. Appl. Chem. 78 (2005) 1948.
[11] (a) A. Kiennemann, R. Kieffer, A. Kaddouri, P. Poix, J.L. Rehspringer, Catal. Today 6 (1990) 409;
(b) P. Chanaud, A. Julbe, A. Larbot, C. Guizard, L. Cot, H. Borges, A. Giroir Fendler, C. Mirodatos, Catal. Today 25 (1995) 225.
[12] A. Marsal, E. Rossinyol, F. Bimbela, C. Tellez, J. Coronas, A. Cornet, J.R. Morante, Sensors Actuators B 109 (2005) 38.
[13] T. Aitasalo, J. Holsa, M. Lastusaari, J. Legendziewicz, L. Lehto, J. Linden, M. Marysko, J. Alloys Compds. 380 (2004) 296.
[14] J. Holsa, M. Lahtinen, M. Lastusaari, J. Valkonen, J. Viljanen, J. Solid State Chem. 165 (2002) 48.
[15] M.R. Esquivel, A.E. Bohe, D.M. Pasquevich, J. Mater. Process. Technol. 170 (2005) 304.
[16] (a) C.W. Koch, A. Broido, B.B. Cunningham, J. Am. Chem. Soc. 74 (1952) 2349;
(b) C.W. Koch, B.B. Cunningham, J. Am. Chem. Soc. 75 (1953) 796.
[17] C. Bungenstock, T. Troster, W.B. Holzapfel, Phys. Rev. B 62 (2000) 7945.
[18] J. Lee, Q. Zhang, F. Saito, J. Solid State Chem. 160 (2001) 469.
[19] D. Elwell, H.J. Scheel, Crystal Growth from High-Temperature Solutions, Academic Press, New York, 1975.
[20] (a) I.P. Parkin, Chem. Soc. Rev. (1996) 199;
(b) E.G. Gillan, R.B. Kaner, Chem. Mater. 8 (1996) 333.
[21] (a) A. Hector, I.P. Parkin, Polyhedron 12 (1993) 1855;
(b) J.B. Wiley, E.G. Gillan, R.B. Kaner, Mater. Res. Bull. 28 (1993) 893;
(c) M.D. Aguas, G.C. Combe, I.P. Parkin, Polyhedron 17 (1998) 49;
(d) E.G. Gillan, R.B. Kaner, J. Mater. Chem. 11 (2001) 1951;
(e) S. Perera, N. Zelenski, E.G. Gillan, Chem. Mater. 18 (2006) 2381.
[22] (a) I.P. Parkin, A.V. Komarov, Q. Fang, Polyhedron 15 (1996) 3117;
(b) E.S. Toberer, J.C. Weaver, K. Ramesha, R. Seshadri, Chem. Mater. 16 (2004) 2194;
(c) J. Gopalakrishnan, T. Sivakumar, K. Ramesha, V. Thangadurai, G.N. Subbannna, J. Am. Chem. Soc. 122 (2000) 6237.
[23] A.T. Rowley, I.P. Parkin, Inorg. Chim. Acta 211 (1993) 77.
[24] D.R. Miller, J. Wang, E.G. Gillan, J. Mater. Chem. 12 (2002) 2463.
[25] R.R. Gupta, in: O. Madelung (Ed.), Landolt–Bornstein New Series: Vol. 16—Diamagnetic Susceptibility, Springer, New York, 1986.
[26] D.R. Lide, Handbook of Chemistry and Physics, 78th ed., CRC Press, New York, 1997.
[27] H.J. Seifert, J. Therm. Anal. Calorim. 82 (2005) 575.
[28] W. Brzyska, E. Swita, Monatsh. Chem. 129 (1998) 1133.
[29] M.R. Esquivel, A.E. Bohe, D.M. Pasquevich, Mater. Res. Bull. 42 (2007) 553.
[30] (a) A.M. De Asha, J.T.S. Critchley, R.M. Nix, Surf. Sci. 405 (1998) 201;
(b) S.-S. Lee, S.-H. Byeon, Mater. Sci. Eng. B 133 (2006) 77.
[31] Y. Katayama, R. Hagiwara, Y. Ito, J. Electrochem. Soc. 142 (1995) 2174.
[32] (a) M. Cardona, L. Ley, Photoemission in Solids 1: General Principles, vol. 26, Springer, Berlin, 1978;
(b) J.C. Fuggle, N. Martensson, J. Electron Spectrosc. Relat. Phenom. 21 (1980) 275.
[33] J.A. Bearden, A.F. Burr, Rev. Mod. Phys. 39 (1967) 125.
[34] M. Schmidt, H. Oppermann, M. Binnewies, Z. Anorg. Allg. Chem. 625 (1999) 1001.
[35] N.T. McDevitt, W.L. Baun, Spectrochim. Acta 20 (1964) 799.

[36] (a) R.M. Silverstein, G.C. Bassler, T.C. Morrill, Spectrometric Identification of Organic Compounds, fifth ed., Wiley, New York, 1991;
(b) NIST Chemistry WebBook, 〈http://webbook.nist.gov/〉, 2006 (accessed April 2007).
[37] (a) I.P. Parkin, A. Hector, J. Mater. Sci. Lett. 12 (1993) 1856;
(b) A.T. Rowley, I.P. Parkin, J. Mater. Chem. 3 (1993) 689;
(c) J.C. Fitzmaurice, I.P. Parkin, A.T. Rowley, J. Mater. Chem. 4 (1994) 285;
(d) P.R. Bonneau, R.B. Kaner, Inorg. Chem. 32 (1993) 6084.
[38] (a) R.S. Tebble, D.J. Craik, Magnetic Materials, Wiley Interscience, New York, 1969;
(b) J.E. Huheey, E.A. Keiter, R.L. Keiter, Inorganic Chemistry Principles of Structure and Reactivity, fourth ed., Harper Collins College Publishers, New York, 1993.
[39] J. Holsa, R.-J. Lamminmaki, M. Lastusaari, P. Porcher, R.S. Puche, J. Alloys Compds. 300–301 (2000) 45.
[40] J. Holsa, M. Lastusaari, J. Niittykoski, R.S. Puche, Phys. Chem. Chem. Phys. 4 (2002) 3091.
[41] P. Caravan, J.J. Ellison, T.J. McMurry, R.B. Lauffer, Chem. Rev. 99 (1999) 2293.
[42] (a) B. Sitharaman, K.R. Kissell, K.B. Hartman, L.A. Tran, A. Baikalov, I. Rusakova, Y. Sun, H.A. Khant, S.J. Ludtke, W. Chiu, S. Laus, E. Toth, L. Helm, A.E. Merbach, L.J. Wilson, Chem. Commun. (2005) 3915;
(b) J.-L. Bridot, A.-C. Faure, S. Laurent, C. Riviere, C. Billotey, B. Hiba, M. Janier, V. Josserand, J.-L. Coll, L. Vander Elst, R. Muller, S. Roux, P. Perriat, O. Tillement, J. Am. Chem. Soc. 129 (2007) 5076.
[43] (a) L.B. Steren, M. Tovar, S.B. Oseroff, Phys. Rev. B 46 (1992) 2874;
(b) H.A. Hoppe, G. Kotzyba, R. Pottgen, W. Schnick, J. Solid State Chem. 167 (2002) 393;
(c) C. Thiriet, P. Javorski, R.J.M. Konings, Solid State Commun. 134 (2005) 409.
[44] J. Holsa, P. Porcher, J. Chem. Phys. 75 (1981) 2108.
[45] S. Areva, J. Holsa, R.-J. Lamminmaki, H. Rahiala, P. Deren, W. Strek, J. Alloys Compds. 300–301 (2000) 218.